Pertanika J. Sci. & Technol. 34 (2): 763 - 786 (2026)

PERTANIKA JOURNALS

SCIENCE & TECHNOLOGY

Journal homepage: http://www.pertanika.upm.edu.my/

Ensemble Docking and Molecular Dynamics Pattern Similarity Analysis for the Discovery of Dengue Virus RNA-Dependent RNA Polymerase Inhibitor

Amaal Mohammed Salih Nasr[1], Mohd Basyaruddin Abdul Rahman[1], Muhammad Alif Mohammad Latif[1,2], Faridah Abas[3], Siti Munirah Mohd Faudzi[1,4], and Bimo A. Tejo[1]*

[1]Department of Chemistry, Faculty of Science, Universiti Putra Malaysia, 43400 UPM Serdang, Selangor, Malaysia
[2]Centre for Foundation Studies in Science, Universiti Putra Malaysia, 43400 UPM Serdang, Selangor, Malaysia
[3]Department of Food Science, Faculty of Food Science and Technology,Universiti Putra Malaysia, 43400 UPM Serdang, Selangor, Malaysia
[4]Natural Medicine and Product Research Laboratory, Institute of Bioscience, Universiti Putra Malaysia, 43400 UPM Serdang, Selangor, Malaysia

ABSTRACT

Dengue fever, transmitted by Aedes mosquitoes, remains a major public health concern across tropical and subtropical regions. The urgent need for effective antiviral agents has drawn significant attention to the NS5 RNA-dependent RNA polymerase (RdRp), a key enzyme required for viral replication. This study aimed to identify promising RdRp inhibitors using ensemble docking, molecular dynamics (MD) simulations, and MD pattern similarity analysis. A 150-ns MD simulation of both the NS5 RdRp apoprotein and its ligand-bound complex was conducted to assess conformational stability and dynamic behaviour. Ligand binding reduced overall protein flexibility, indicating stabilising interactions suggestive of inhibitory activity. Structural and dynamic features were examined through RMSF, SASA, Rg, and dynamic cross-correlation matrix (DCCM) analyses, which collectively revealed distinct residue correlation patterns upon ligand binding. Clustering of the MD trajectories generated 225 representative conformations, 138 from the apoprotein and 87 from the complex used for ensemble docking of 328 curcuminoid compounds. ADMET analysis further showed that compounds 1CJS and 90 possessed favourable absorption and metabolic properties, with low predicted toxicity. Among all screened ligands, compound 90 demonstrated the strongest binding affinity.

ARTICLE INFO

Article history:
Received: 03 September 2024
Accepted: 10 December 2025
Published: 17 April 2026

DOI: https://doi.org/10.47836/pjst.34.2.08

E-mail addresses:
gs59663@student.upm.edu.my (Amaal Mohammed Salih Nasr)
basya@upm.edu.my (Mohd Basyaruddin Abdul Rahman)
aliflatif@upm.edu.my (Muhammad Alif Mohammad Latif)
faridah_abas@upm.edu.my (Faridah Abas)
sitimunirah@upm.edu.my (Siti Munirah Mohd Faudzi)
bimo.tejo@upm.edu.my (Bimo A.Tejo)
* Corresponding author

e-ISSN: 2231-8526

Subsequent MD simulations confirmed its stable binding mode and favourable dynamic profile. MD pattern similarity analysis also showed that compound 90 closely mimics the structural and dynamic behaviour of the native ligand GTP, supporting its potential as a potent RdRp inhibitor. Overall, these findings highlight compound 90 as a promising curcuminoid derivative for further development of antiviral agents against the dengue virus.

Keywords: Drug resistance, dengue, molecular docking, molecular dynamics, RdRp, structure-based drug discovery, virtual screening

INTRODUCTION

Dengue virus (DENV), a Flavivirus genus member, poses a major global health threat with four serotypes (DENV-1 to DENV-4) sharing 60%-70% amino acid identity. Each serotype includes distinct genotypes with less than 3% sequence variation (Weaver & Vasilakis, 2009). The virus carries a ~11 kb positive-sense, single-stranded RNA genome that encodes a single open reading frame (ORF) flanked by 5' and 3' untranslated regions, as shown in Figure 1 (Khetarpal & Khanna, 2016). This ORF translates into 10 proteins: three structural (C, E, prM) and seven non-structural (NS1-NS5). Structural proteins play a crucial role in the virus's assembly, maturation, and entry into the host cell by forming the capsid and viral envelope (Qureshi, 2020). In contrast, non-structural proteins are essential for sustaining the viral life cycle, as they facilitate RNA replication, enzymatic processing, and immune evasion. Additionally, non-structural proteins can remodel specific host cellular pathways to enhance viral infection. These coordinated functions are vital for the successful replication of the dengue virus.

Due to their role in RNA virus replication, RNA-dependent RNA polymerases (RdRps) serve as crucial anti-viral drug targets (Singh et al., 2020). They generate viral

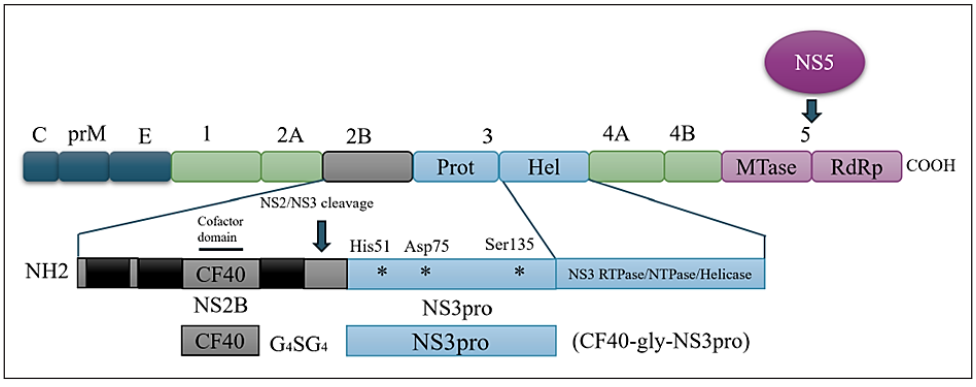

Figure 1. Schematic representation of the genome of DENV, consisting of structural (capsid (C); membrane (M); envelope (E); and non-structural (NS1-NS5) proteins

RNA using an RNA template, catalysed by conserved catalytic residues such as Trp795, Thr794, Ser710, and Arg729, directly interacting with GTP Figure 2 (Yap et al., 2007). These residues are essential for catalysis and substrate recognition. Lim et al. (2018) also identified an allosteric "N-pocket" at the thumb/palm interface, in addition to the active site, using fragment-based crystallographic screening. Fragment-based optimisation of portions of the molecules that address these regions led to potent inhibitors of biphenyl acetic acid. This two-site mechanism offers more options for developing antiviral therapy and further explores the space of RdRp druggability.

Currently, no specific antiviral drugs have been approved for the treatment of dengue. The current management of dengue primarily involves supportive care, such as hydration and fever management, rather than targeting the virus directly. This gap underscores the urgent need for effective antiviral agents that can directly inhibit the replication of DENV.

Due to their ability to target various biological processes without side effects, curcuminoids have attracted therapeutic interest in treating immune, metabolic, and cancer diseases (Mahmood et al., 2015; Siviero et al., 2015). These curcuminoids have demonstrated antibacterial (Prlina et al., 1958), antimalarial (Prlina et al., 1958), diuretic (Douglas & Rubin, 1961), antirheumatic (Markham, 2017) and antiretroviral activities (Adkins & Faulds, 1998). The term "curcuminoids" is the appropriate choice because the context suggests a broader examination of the therapeutic potential of turmeric-derived compounds rather than focusing solely on curcumin.

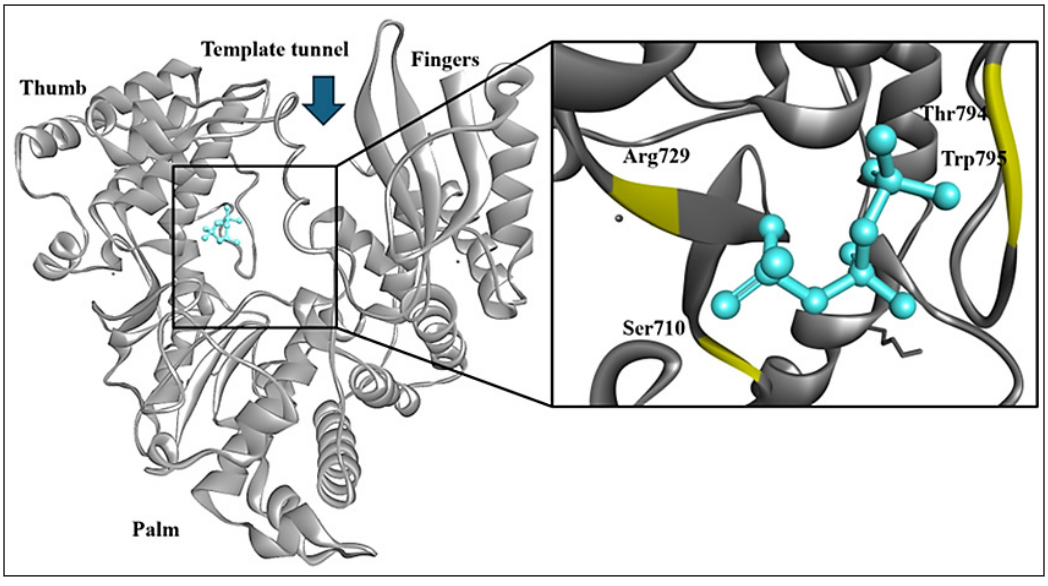

Figure 2. The RdRp enzyme's essential elements and active site

Curcuminoids are increasingly recognised as promising inhibitors of dengue virus, as they can target both viral proteins and host pathways essential for viral replication. Several studies show that curcumin and its derivatives inhibit the dengue NS2B-NS3 protease by binding to an allosteric pocket and disrupting the β-hairpin structure required for enzymatic activation, ultimately blocking viral polyprotein processing (Lim et al., 2020). Curcuminoid analogues have also demonstrated stronger antiviral activity than curcumin by suppressing lipid-biosynthesis genes such as ACC and FAS and by interfering with actin polymerisation, a key process for viral entry and intracellular movement (Balasubramanian et al., 2019). Curcumin additionally reduces DENV-2 plaque formation at non-toxic levels, supporting its potential as a safe antiviral scaffold (Padilla-S et al., 2014). The potential of curcuminoids as dengue RdRp inhibitors remains largely unexplored.

This study uniquely integrates ensemble docking with MD pattern similarity analysis to identify dengue RdRp inhibitors from our curcuminoid collection. By screening 328 curcuminoid compounds against multiple RdRp conformations from a 150-ns MD simulation, we accounted for the protein's dynamic flexibility. Top ligands were evaluated using RMSD, RMSF, Rg, and DCCM to assess their dynamic similarity to the native ligand GTP. This dual approach enhanced the accuracy of identifying strong binders with GTP-like behaviour. Arg729 and Trp795 emerged as key anchors in stabilising lead compounds. Additionally, the application of curcuminoids created a new chemical area for antiviral targeting.

METHODOLOGY

Target Protein and Ligand Preparation

The three-dimensional crystallised structure of DENV RdRp complexed with GTP (PDB ID: 2J7U) was taken from the Protein Data Bank (Berman et al., 2000) and processed using Play-Molecule Protein-Prepare web service to have it ready for molecular dynamics (MD) simulations (Martínez-Rosell et al., 2017). The web platform facilitates the automation of the addition of hydrogen atoms, removal of crystallographic water molecules, a nd adjustment of the protonation state, to ensure chemical accuracy. It also clears up typical structure problems, such as the disulfide bond recognition and the absence of the side chain, adjusts disulfide bonds, pH, and the concentration of ions in a customisable way. Through the optimisation of the structure, the model becomes applicable to the accurate simulation of the behaviour of small molecules and, more in-depth analysis of the interaction of ligands can be undertaken as well as creating high-quality conformational ensembles.

Molecular Dynamics Simulations

The RdRp was simulated in an apoprotein and GTP-bound state using AMBER14 force field (Maier et al., 2015) implemented in YASARA Structure (v21.12.19) (Krieger & Vriend, 2015).

The simulations used the Particle Mesh Ewald technique of accurate long-range electrostatics and periodic boundary conditions at 300 K and 0.9% NaCl. Solvation was done in a cubic simulation cell extended 20 Å beyond the protein surface. Temperature in the model was controlled with the help of a Berendsen thermostat to maintain system stability throughout the simulation.

The protein complex underwent a thorough preprocessing scenario prior to the simulation, during which fixing of energy by the use of steepest decline algorithm on 5000 cycles and the cleaning of structures (Brooks et al., 1983) were used in attaining stable conformation and broadening saddles (Hassan et al., 2022). A 1.25 fs time step was used to model the simulations, with a 100 ps interval used to record the trajectories. Analyses were conducted by utilising the default macro md_analyse.mcr to verify the system's structural stability and dynamic characteristics.

Generation of Ensemble Structure

The ensemble structures were constructed by clustering protein conformations by backbone RMSD with a cutoff of 2.0 Å using the YASARA macro md_analyse.mcr. This generated 225 clusters, with 87 deriving from the RdRp complex and 138 from the apoprotein. In the case of ensemble docking, every cluster was identified by representative structures and saved in PDB format. The 150-ns production MD simulations were performed in duplicate, aimed at determining the structural changes induced by the ligand, and to represent conformational diversity of both unbound and bound forms. The dynamic stability of proteins and ligand binding flexibility were comprehensively understood due to this dual strategy.

Ligand Preparation

OpenBabel (O'Boyle et al., 2011) was used to convert ligand structures into SDF format. The ligands were subjected to a 20-step conjugate gradient minimisation after a 200-step steepest descent minimisation with a step size of 0.02 using YASARA Structure (Krieger & Vriend, 2015).

Protein-ligand Molecular Docking

This study tested 328 curcuminoid compounds from the Universiti Putra Malaysia (UPM) natural product collection against the dengue virus RdRp. After ligand preparation, 225 representative RdRp conformations produced by clustering analysis and molecular dynamics simulations were used for ensemble docking. Docking grids were established using known active site coordinates, and these conformers, which represented apoprotein and ligand-bound states, were aligned and superimposed to preserve uniform orientation.

Using the Lead Finder engine in Standard Precision mode, which is tuned for quick, high-throughput screening, virtual screening was carried out in Cresset Flare (v5.0.0). The approach was designed to balance speed and accuracy in order to evaluate big libraries efficiently. An Intel® Core™ i5-11300H CPU, 16 GB of RAM, and a 64-bit operating system was used for all calculations. For every ligand, docking results yielded virtual screening (VS) scores and binding free energies (ΔG). To evaluate their potential as RdRp inhibitors, top-scoring compounds were chosen for additional examination of binding interactions, stability, and MD-based dynamic similarity to GTP (Stroganov et al., 2009).

Evaluation of Drug-like Properties using ADME Analysis

After completing the docking study, we analysed the selected compounds using the SwissADME web tool (https://www.swissadme.ch/) to evaluate their drug-like properties. This allowed us to check their stability, solubility, absorption, metabolism, and potential toxicity. The compounds' chemical structures were first converted into SMILES format using Open Babel, which is required for the analysis. This step helped us understand how the compounds might behave in the human body and identify the most promising candidates for further study.

Molecular Dynamics Simulations of Selected Curcuminoids

After ensemble docking, molecular dynamics (MD) simulation was used to determine the stability of high-ranking ligand-protein complexes and investigate the effect of ligand-induced binding on RdRp structural dynamics under close to physiological settings. MD simulations were carried out with the AMBER14 force field implemented in YASARA Structure (version 21.12.19) with the simulation duration of 150 ns. At 300 K, the systems were solvated in a TIP3P water box with 0.9% of NaCl. To critically assess stability and strength of interactions, analyses were carried out on radius of gyration (Rg), dynamic cross-correlation matrix (DCCM), estimation of binding free energy through MM/PBSA, root mean square deviation (RMSD) and root mean square fluctuation (RMSF).

RESULTS AND DISCUSSION

Molecular Dynamics Simulations

The present work has generated an ensemble of RdRp conformations used in conducting structure-based virtual screening using molecular dynamics (MD) simulation. These simulations based upon the AMBER14 force field implemented in YASARA Structure proved the dynamic features of the RdRp over a time of 150 ns. To model physiological conditions, the simulation environment was made up of explicit water and 0.9 % NaCl at a temperature of 300 K. The essence of the ensemble docking strategy was extracting

appropriate representative conformations and proteins in the generated trajectories through clustering analysis. These different conformers allowed more accurate docking because they considered the receptor's conformational flexibility, which is usually ignored in the single-structure docking methods.

Conversion of Trajectory Data into Conformational Ensemble

Obtaining the ensemble of the conformations of proteins through molecular dynamics (MD) trajectory data is essential to depict how proteins change their structure over time. The conformations were analysed using YASARA command md_analyse.mcr, and then clustered by backbone RMSD values. Applying this clustering method, two protein variations were represented with 225 distinct conformations, including 87 conformations of the RdRp complex and 138 conformations of the apoprotein. An RMSD cutoff was set at 2.0 Å to ensure we only grouped structurally similar frames. This permitted a systematic study of the dynamics of the protein.

To maintain diversity within the clusters, a minimal separation ('rmsdmin') of 2.0 A was set between structural positions of each pair of the sample structures. The dataset was structurally unique because each cluster was represented by one single conformation stored as "Protein_cluster*yob". Such a criterion allowed a rich set of structural motifs to be expressed and played a part in establishing a large but non-redundant set of conformational states. Due to such a process, the apoprotein and ligand-bound RdRp conformational landscapes were resolved considerably, allowing more accurate subsequent analysis, such as ensemble docking.

Molecular Docking

Ensemble docking employed Cresset Flare (v5.0.0) designed to employ the XED polarisable force field. A total of 225 MD-derived RdRp structures were prepared and superimposed for docking. Docking was performed using the Lead Finder algorithm with a grid box centred on the native ligand’s binding site. All 328 curcuminoid compounds were parameterised using the GAFF2 AMBER force field to evaluate their inhibitory potential against DENV RdRp (Brooks et al., 1983).

Several compounds, i.e., 90, 175, 1CJS, 3DDX, 113, and 187 demonstrated stronger binding affinities than GTP and interacted with key catalytic residues, highlighting them as promising inhibitors. These compounds satisfied two critical criteria: superior binding strength and direct engagement with functional sites. The Lead Finder Virtual Screening (LF VSscore) was used for initial ranking (Stroganov et al., 2009), where more negative scores indicated stronger predicted interactions. This scoring helped prioritise top candidates for deeper analysis, including MD simulations and MM/PBSA calculations.

Table 1 summarises the binding affinities of compounds 90, 175, 1CJS, 3DDX, 113, and 187, with compound 90 exhibiting the strongest affinity compared to the others, including GTP. Table 2 details the molecular interactions of these high-affinity compounds with critical residues within the active site of RNA-dependent RNA polymerase (RdRp). Specifically, compounds 90, 175, 1CJS, 3DDX, 113, and 187 show consistent and specific binding to essential catalytic residues such as Arg729, Ser710, Thr794, Trp795, and Arg737, along with neighbouring amino acids that contribute to the structural and functional stability of the active site. The interaction patterns involve hydrogen bonding, electrostatic contacts, hydrophobic interactions, and π–π stacking, which act synergistically to stabilise the ligands and enhance their binding affinity.

Notably, Ser710 and Thr794 frequently form hydrogen bonds that help maintain the correct orientation of the ligand within the binding pocket. Arg729 and Arg737 engage in electrostatic interactions with polar functional groups on the ligands, strengthening their anchorage and contributing to overall binding energy. Trp795 often participates in π–π stacking interactions with aromatic moieties of the ligands, which is particularly important for stabilising planar and conjugated chemical scaffolds. Collectively, these interactions highlight the ability of the selected compounds to form stable and favourable contacts with RdRp, supporting their potential as effective inhibitors that may interfere with its enzymatic function.

In Figure 3, the best binding position of compound 1CJS in RdRp is represented with a docking score of -10.9 kcal/mol, depicting the interaction between RdRp and compound 1CJS at the major interacting residues in the binding pose. A pose view was utilised to gain insights into the residues responsible for the negative free energy. The key residues involved were Thr794, Arg729, Thr758, Ser710, Ser796, Ser791, Met761, Thr766, Thr793, Gln742, Leu734, Trp762, Met765, Ile740, and Cys709. Further analysis of the nonbonded interactions revealed that compound ICJS formed strong hydrogen bonds with the interacting residues Thr766, Arg729, Ser796, Cys709, and His711. Additionally, alkyl interactions with Arg737, Arg792, and Leu511 indicated the interaction of RdRp and compound 1CJS with the active site of the RdRp main protease.

In Figure 4, the compound ligand 175 demonstrated a scoring binding pose in RdRp with a score of -11.2 kcal/mol, highlighting the interaction between RdRp and the compound ligand 175 at the major interacting residues in the binding pose. A pose view was utilised to gain insights into the residues responsible for the negative free energy. The key residues involved were Thr794, Arg729, Thr758, Arg792, Ser710, Ser796, Ser741, Met761, Thr766, Thr793, Gln742, and Leu734. Further analysis of the nonbonded interactions revealed that compound 175 formed strong hydrogen bonds with the interacting residues Thr794 and Arg729. Moreover, alkyl and pi-alkyl interactions with Trp795, Ile740, Tyr758, His711, and Leu511 indicate the interaction of RdRp and compound 175 with the active site of the RdRp main protease.

Table 1
Docking results with the highest docking energies

Structure	ID	LF Vsscore (kcal/mol)
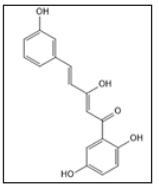	90	-11.8
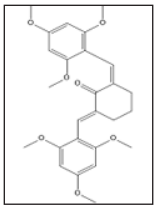	175	-11.2
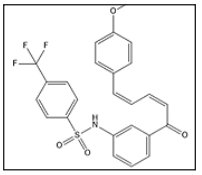	ICJS	-10.9
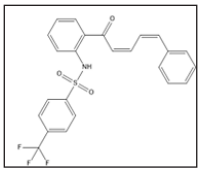	3DDX	–10.4
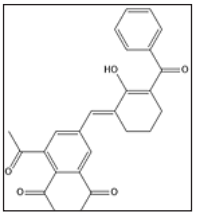	113	-10.3
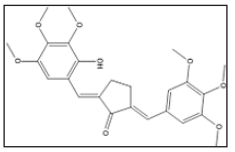	187	-10.3
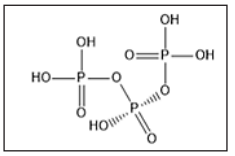	GTP (control)	- 6.9

Note. The compound IDs represent different curcuminoid compounds. The LF Vsscore values indicate the predicted binding energies obtained from molecular docking simulations, where more negative values correspond to stronger predicted binding affinity. GTP was included as a control ligand for comparison

Table 2
Types of interactions between the top 3 molecular compounds with the highest binding affinities and the RdRp residues, with the original GTP ligand used as a positive control

ID	Hydrogen Bond Interaction	Pi-Pi T Shaped Interaction	Halogen Interaction	Pi-Alkyl Interaction	Pi-Sulphur /Anion	Carbon-Hydrogen Interaction	Pi-Pi Stacking
90	Thr793 Leu734 Cys709	Thr766		Met761 Cys709	Cys709	Arg737	Thr794
1CJS	Trp762 Thr794		Cys709 Ser710 His711	Arg737 Trp803 Leu511	Met761 Met765	Ser710 His711 Leu734 Ser796	
175	Tyr758 Arg792 Trp795 Arg729	His711 Trp795		His711 Trp705 Tyr758		Arg729 Cys709 Arg737	
GTP	Trp795 Arg729 Arg737					Thr794	

Note. The table summarises the types of non-covalent interactions between the top three curcuminoid compounds with the highest predicted binding affinities and dengue RdRp residues, with GTP included as a positive control. Interactions include conventional hydrogen bonds, Pi-Pi T-shaped, halogen, Pi-alkyl, Pi–sulfur/anion, carbon-hydrogen, and Pi–Pi stacking interactions. These interactions indicate how each compound stabilises within the active site and contributes to the overall binding affinity

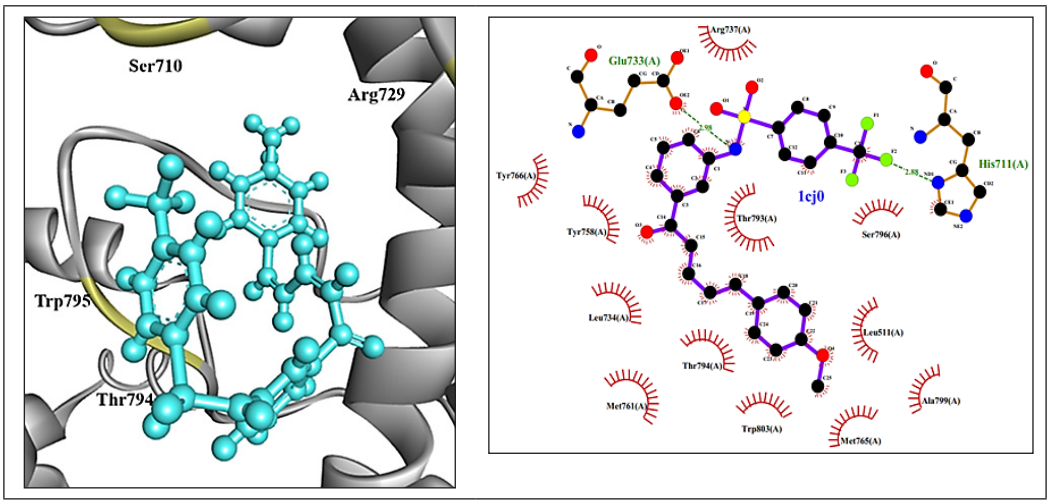

Figure 3. Residues at the active site of RdRp that interact with compound1CJS. Conventional H-bonds (green dashed line) are shown

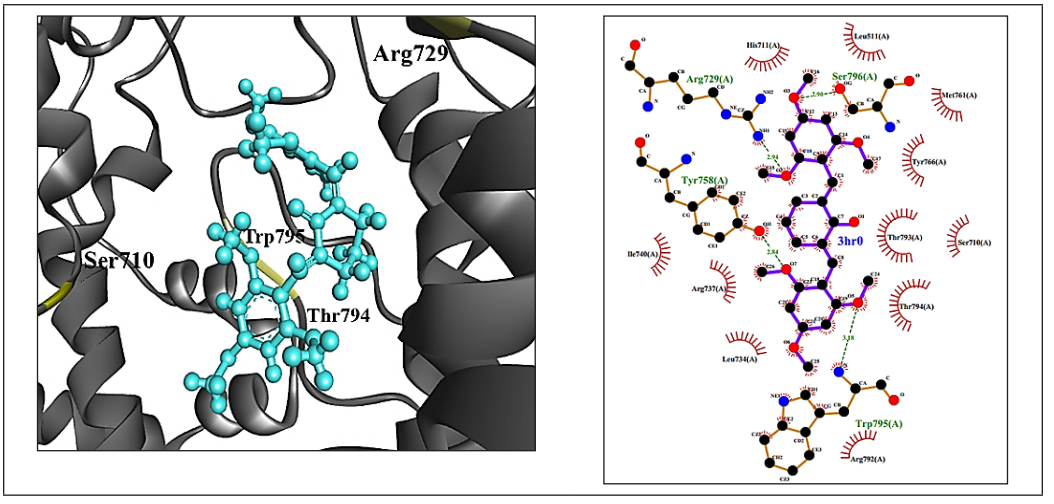

Figure 4. Residues at the active site of RdRp that interact with compound175. Conventional H-bonds (green dashed line) are shown

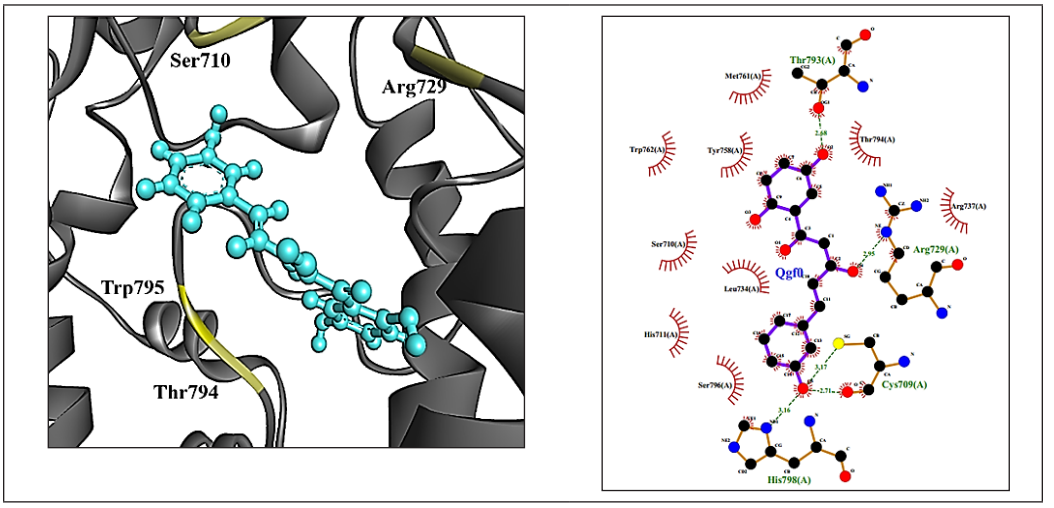

Figure 5. Residues at the active site of RdRp that interact with compound 90. Conventional H-bonds (green dashed line) are shown

As illustrated in Figure 5, compound 90 demonstrated the most favourable binding pose within the RdRp active site, achieving a docking score of -11.8 kcal/mol, indicative of strong binding affinity. The interaction was stabilised by a network of key amino acid residues, including Thr794, Arg729, Thr758, Ser710, Met761, Thr766, Thr793, Tyr606, Gly662, Ser661, Cys706, Leu734, Glu733, His798, and Leu511, which collectively formed a well-defined binding environment. A closer examination of non-bonded interactions revealed that compound 90 established multiple hydrogen bonds with Thr794, Thr793, Cys709,

Ser661, and Thr766, enhancing the specificity and strength of binding. Additionally, pi-alkyl interactions with Arg737 further contributed to the stability of the ligand-protein complex. These findings strongly suggest that compound 90 effectively occupies and interacts with the RdRp catalytic site, potentially interfering with its enzymatic function.

ADMET Analysis

ADMET, which stands for Absorption, Distribution, Metabolism, Excretion, and Toxicity, is an essential part of drug development. It helps us understand how a compound behaves in the human body; how well it is absorbed, where it goes, how it is broken down, how it is eliminated, and whether it might be toxic. Studying these properties early on makes it easier to identify promising drug candidates and avoid problems later in development.

Table 3 shows notable differences among the five compounds in terms of drug-likeness, solubility, and predicted oral absorption. Compounds 90 and 1CJS show the most favourable overall profiles, combining suitable molecular weight, good solubility, and high gastrointestinal absorption. Compound 1CJS emerges as the strongest candidate, as it has no PAINS or Brenk alerts and exhibits no major metabolic or permeability issues. Compound 90 also performs well, though the presence of several structural alerts suggests careful consideration. Compound 175 remains acceptable, with moderate drug-likeness, but its CYP2D6 inhibition slightly reduces its appeal. In contrast, compounds 3DDX and 133 demonstrate poor solubility, low absorption, and excessive lipophilicity, making them less suitable as lead compounds. Among them, Compound 133 is the weakest, showing additional P-gp substrate behaviour and a Lipinski rule violation. Overall, Compounds 90 and 1CJS appear to be the most promising ADME candidates for further optimisation and experimental evaluation.

MD Simulations

Molecular dynamics (MD) simulations were performed after the docking analysis to take solvent effects into consideration and assess the structural stability of the resultant ligand-protein complexes. The simulations reported that conformation relaxation of the ligand associated with an induced-fit process occurs after binding, and the RdRp receptor was also rearranged. The explicit inclusion of the water molecules in the modelled environment allowed a deeper comprehension of the solvent-mediated interactions and destabilisation and stabilisation of complexes. To a large extent, we were able to assess the stability and dynamic behaviour of the ligand-receptor complexes under near physiological conditions more realistically due to our solvent-aware methodology.

More so, the simulation provided valuable data regarding the system's evolution by providing a dynamic picture of the complex. In this dynamic view, a complete vision of the behaviour and interaction of the system is obtained since it becomes easier to differentiate docked and unstable conformations.

Table 3
ADME analysis of the selected compound with the highest binding affinity

Properties	175	3DDX	133	90	1CJS
Physicochemical					
Molecular Weight (g/mol)	451.61	487.49	457.46	298.29	416.47
Log P (Consensus)	4.35	5.32	5.42	2.34	3.99
TPSA (Å²)	72.45	80.85	71.62	97.99	88.51
Water Solubility (Log S ESOL)	-5.48 (Mod. (Soluble)	-6.26 (Poorly Soluble)	-6.53 (Poorly Soluble)	-3.88 (Soluble)	-4.73 (Mod. Soluble)
Pharmacokinetics					
GI Absorption	High	Low	Low	High	High
BBB Permeant	No	No	No	No	No
P-gp Substrate	No	No	Yes	No	No
CYP2D6 Inhibitor	Yes	No	No	No	No
CYP3A4 Inhibitor	No	Yes	No	No	Yes
Drug Likeness					
Lipinski Violations	0	0	1 (Log P)	0	0
Bioavailability Score	0.55	0.55	0.55	0.56	0.56
Alerts					
PAINS/Brenk Alerts	2 Alerts	2 Alerts	2 Alerts	4 Alerts	0 Alerts

Note. Physicochemical properties include molecular weight, Log P, TPSA, and water solubility. Pharmacokinetic properties cover gastrointestinal absorption, blood-brain barrier (BBB) permeability, P-gp substrate status, and CYP450 enzyme inhibition. Druglikeness is assessed based on Lipinski's rules and bioavailability score, while PAINS/Brenk alerts indicate potential structural liabilities. Compounds with optimal ADME profiles and minimal alerts are considered more favourable for drug development

Root Mean Square Deviation

To determine the stability of the structure and dynamics of RdRp complexes with the three best curcuminoid compounds, 150-ns molecular dynamics (MD) simulations were carried out (Figure 6). The root mean square deviation (RMSD) analysis was done to normalise the deviations of the changed structure with the initial structure allowed an impression of how each ligand impacts the consequences of the conformational moves in the RdRp. The simulations showed that the phenomenon of ligand binding led to individual dynamic reactions, showing the differences in the interaction of various ligands with the transformation of the structure of the RdRp.

There was a close match between the RMSD trajectories of compound 90 and that of the native ligand GTP during 70 to 100 ns, suggesting similar orientation in binding to the active site. Both systems showed similar structural dynamics, indicates a possible role of compound 90 as an analogue of GTP. In contrast, compounds 175 and 1CJS maintained consistently low RMSD values (below 3 Å) throughout the simulation, reflecting minimal

conformational fluctuations and high complex stability. Such rigidity may indicate that these compounds lock RdRp into a less flexible, possibly inactive conformation.

The unbound (apoprotein) RdRp also displayed relatively low RMSD values, confirming its inherent structural stability. However, both GTP and compound 90 induced slightly greater rigidity compared to the apoprotein form, which may correspond to the stabilisation of catalytically unfavourable states. Collectively, these findings suggest that curcuminoid-based inhibitors, particularly compound 90, can effectively modulate RdRp dynamics either by mimicking natural substrates or by imposing structural constraints. This reinforces their potential as promising antiviral candidates targeting DENV RdRp.

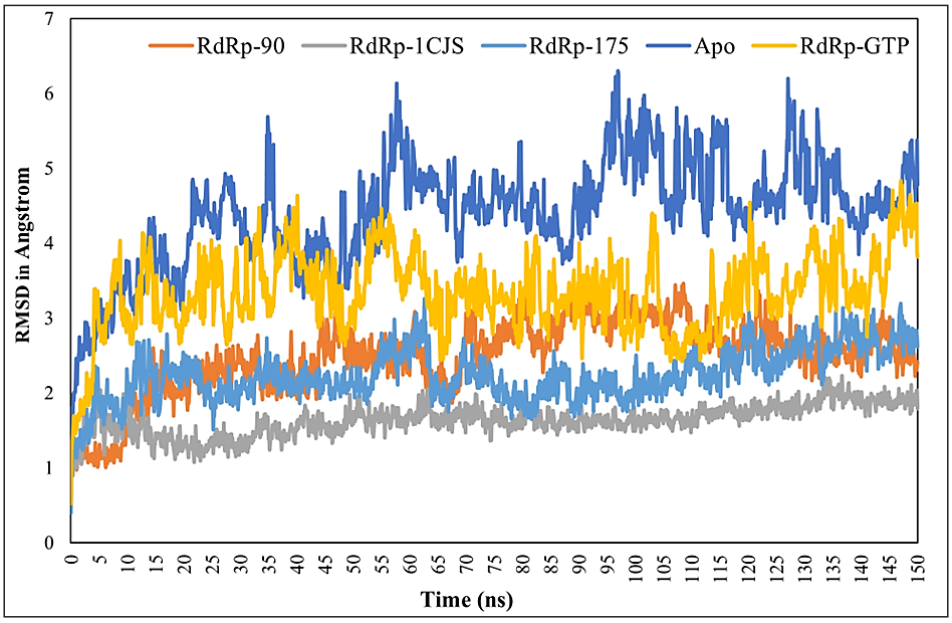

Figure 6. RMSD of complexes of RdRp over the 150 ns time scale

Root Mean Square Fluctuation

The root mean square fluctuation (RMSF) analysis offers critical insights into how ligand binding modulates the flexibility of DENV RdRp (Figure 7). In the unbound (apoprotein) form, the loop spanning residues 341-347, particularly residue 345, exhibited the highest flexibility (RMSF > 5 Å), indicating structural instability near the template tunnel. GTP binding markedly reduced fluctuations in this region, stabilising the loop. Notably, compound 90 elicited a comparable dampening effect, suggesting it mimics GTP's stabilising influence. In contrast, 1CJS and compound 175 produced only modest reductions in flexibility, reflecting weaker or less specific interactions with this region.

At the catalytic site, GTP and compound 90 both significantly reduced the flexibility of residues Ser710, Thr794, and Trp795, indicating strong and stabilising interactions essential for polymerase function. Conversely, compound 175 increased fluctuations at Trp795, suggesting possible destabilisation at a key catalytic position. Additionally, the segment spanning residues 472-486 displayed increased flexibility across all ligand-bound systems, possibly due to ligand-induced allosteric effects. The region Phe348-Arg352 exhibited over 50% reduced fluctuation in all complexes, indicating enhanced conformational stability and potentially improved catalytic precision. Meanwhile, the Thr585-Ser593 segment remained consistently stable, underscoring its likely role as part of the structural core. Collectively, these findings highlight compound 90's ability to replicate GTP's stabilising effect on RdRp dynamics, supporting its potential as a viable inhibitory candidate.

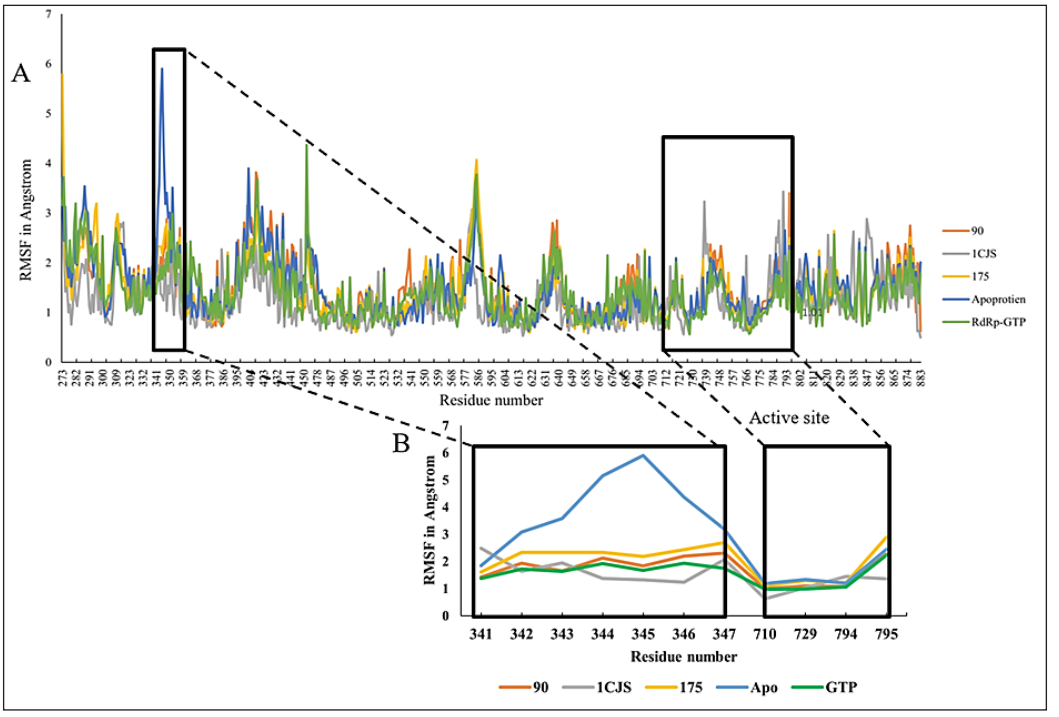

Figure 7. (A) Root mean square fluctuation (RMSF) profile of the RdRp-ligand complexes; (B) Highlighted regions of interest in the RMSF plot

Radius of Gyration

The radius of gyration (Rg)is a significant parameter in the analysis of protein compactness and structural stability in molecular dynamics analyses. Low Rg values characterise more compact and folded protein structures, and high values represent high flexibility or

non-compactness with a partial unfolding. Rg analysis was done in this study to study the relationship between the curcuminoid binding and the structural stability of DENV RdRp.

The ligand-bound RdRp complexes were consistently found to have a lower Rg than the unbound (apoprotein) form, consistent with the idea that binding ligands creates a more stable and compact protein conformation (Figure 8). Two of the tested compounds, GTP and compound 90, possessed almost the same Rg profiles (25.3-26.5 Å), meaning that Compound 90 almost perfectly mimics the RdRp folded architecture of GTP. Compounds 1CJS and 175 also contributed to structural stabilisation, albeit to a lesser extent. In contrast, the apoprotein RdRp showed greater Rg fluctuations, reflecting reduced conformational rigidity. These findings reinforce compound 90's potential to stabilise the polymerase structure similarly to the native ligand, supporting its candidacy as a potent RdRp inhibitor.

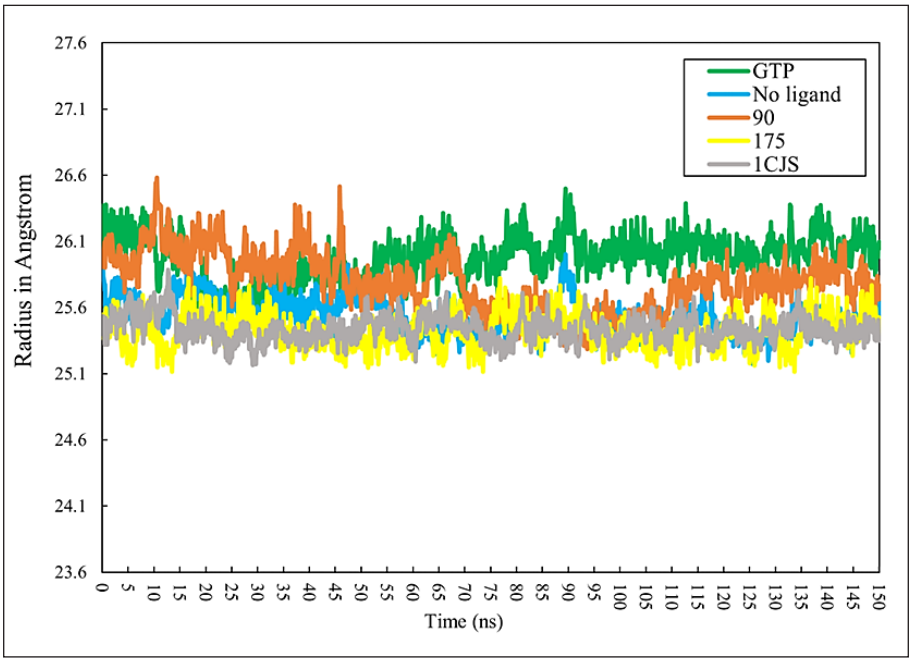

Figure 8. Analysis of the radius of gyration of the RdRp complexes over a 150 ns duration

Dynamic Cross-correlation Matrix

The dynamic cross-correlation matrix (DCCM) analysis of DENV RdRp illustrates how ligand binding modulates internal residue-residue motions during molecular dynamics simulations (Figure 9). In these plots, yellow regions indicate positively correlated, coordinated motions, while blue regions reflect anti-correlated, opposing movements. The red circle highlights the catalytic active-site region, where ligand binding exerts the

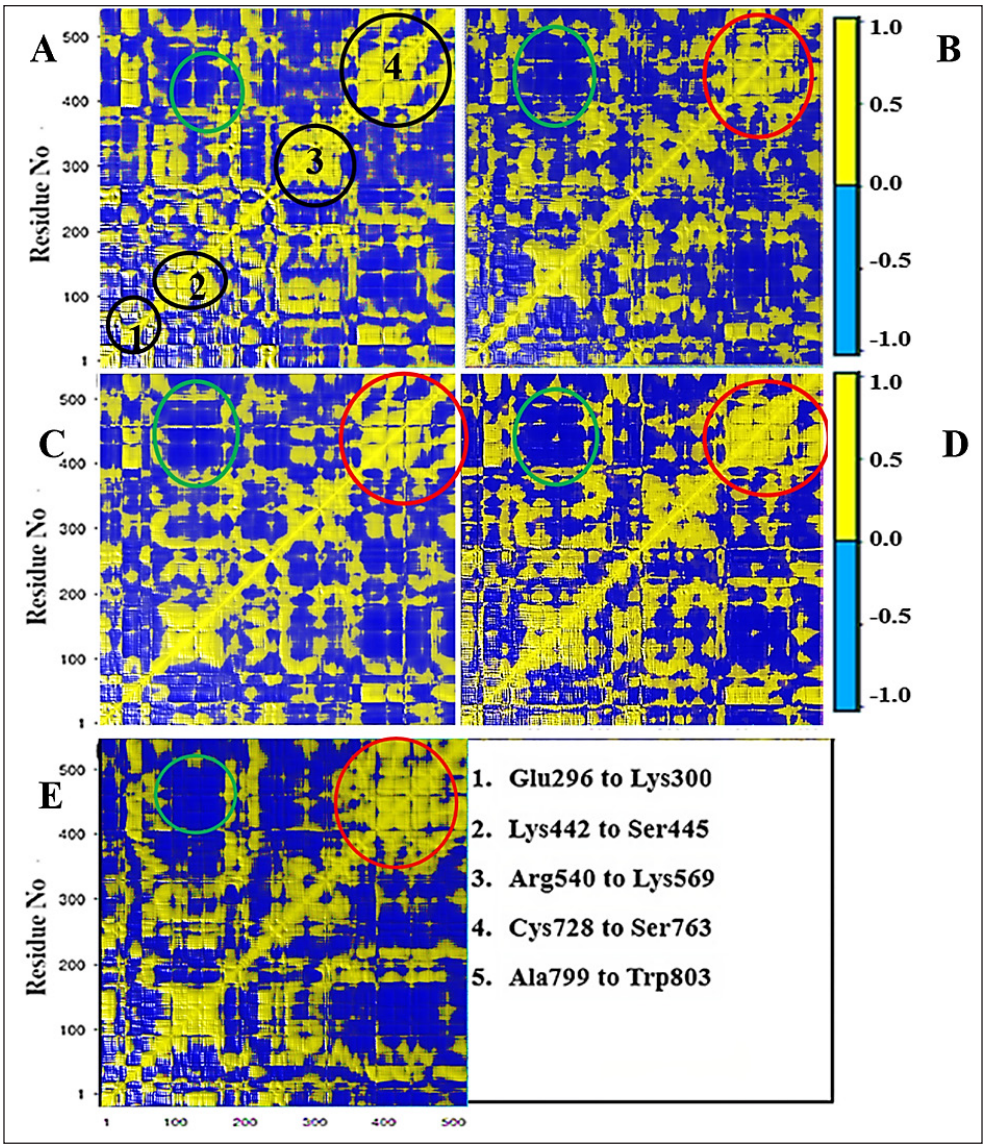

Figure 9. Dynamic cross-correlation map (DCCM) comparing the unbound RdRp structure with its various ligand-bound complexes

greatest influence, and the green circle marks an adjacent residue cluster that supports catalytic stability and intra-protein communication.

In the GTP-bound RdRp (Panel A), four key regions Lys300-Glu296, Lys442-Ser445, Arg540-Lys569, and Cys728-Ser763 exhibited strong positive correlations around both circles, reflecting well-organised dynamics that support efficient RNA synthesis. Compound 90 (Panel C) closely mimicked this pattern, restoring coordinated motions in the

same regions, suggesting that it not only occupies a similar binding pose as GTP but also replicates its effect on RdRp dynamics, supporting its potential as a competitive inhibitor.

Conversely, compound 175 (Panel B) disrupted these correlations, particularly within the catalytic region, weakening residue coordination, whereas 1CJS (Panel D) provided intermediate stabilisation. Notably, both 175 and 1CJS introduced shifts in anti-correlated interactions, especially in regions Cys728-Ser763 and Ala799-Trp803, toward positive correlations, indicating possible allosteric modulation that may stabilise RdRp in a more rigid, less catalytically active conformation. The apoprotein form (Panel E) displayed fragmented and weak correlations, emphasising the critical role of ligand binding in maintaining the structural and functional integrity of the polymerase.

Principal Component Analysis

The principal component analysis (PCA) results for compounds 175, 90, 1CJS, and the native ligand (GTP) are shown in Figure 10. In each subplot (A, B, C, and D), red dots represent positive conformations, i.e. trajectory frames that project in the positive direction along the principal component axis. These conformations correspond to one extreme of the dominant motion captured by PCA and are typically associated with an activated or open functional state of the protein. Conversely, blue dots represent negative conformations, projecting in the negative direction along the same axis, often reflecting a more compact, closed, or inactive structural state.

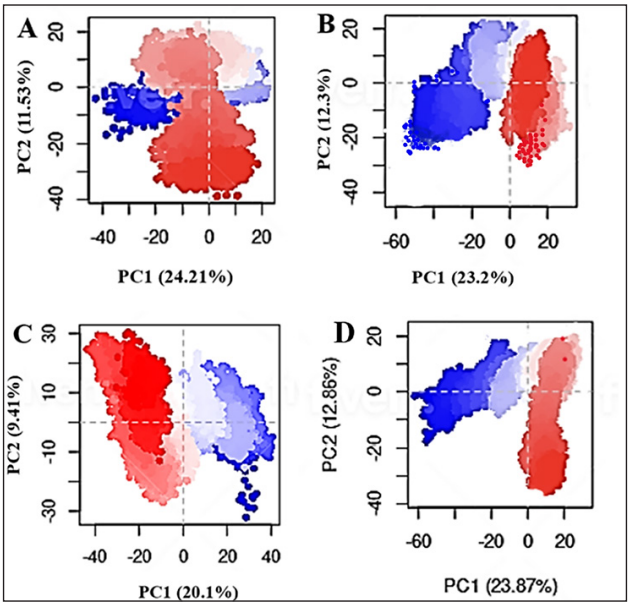

Figure 10. PCA analysis of the curcuminoids compound, where A represents compound 175; B represents compound 90; C represents compound 1CJS; and D represents the native ligand

Principal component analysis (PCA) revealed varying degrees of structural flexibility among the compounds. Compound 175 (Plot A) showed moderate conformational diversity with PC1 and PC2 explaining 24.21% and 11.53% of the variance, respectively. Compound 90 (Plot B) exhibited more pronounced clustering and separation, with PC1 and PC2 accounting for 23.2% and 12.3% respectively, indicating greater structural variation. Compound 1CJS (Plot C) explored a narrower conformational space, with lower variance explained (20.1% and 9.41%), suggesting restricted dynamics.

The native ligand GTP (Plot D) displayed distinct structural states, with PC1 and PC2 contributing 23.87% and 12.86%, respectively, resembling the variation seen with compound 90. Among all, compound 90 and GTP showed the highest structural diversity, while 1CJS remained the most conformationally constrained. Compound 175 showed intermediate behaviour. These findings highlight compound 90's dynamic flexibility, closely mimicking the native ligand's conformational behaviour, which may enhance its inhibitory potential.

Binding Free Energy Analysis

We employed the molecular mechanics/Poisson-Boltzmann surface area (MM/PBSA) method for binding free energy calculations using YASARA Structure and AMBER14 force field. MM/PBSA accurately estimates the binding free energies and obtains valuable information concerning interactions between the ligands and receptors. The binding free energy (DGbind) in kcal/mol was calculated by using the following formula:

$$\Delta Gbind = \Delta Gcomplex\ (minimised) - (\Delta Gligand\ (minimised) + \Delta Greceptor\ (minimised)$$

In the case that ΔGreceptor complex (minimised) is the minimised energy of the complex, ΔGreceptor ligand (minimised) is the minimised energy of the isolated ligand, and ΔGreceptor receptor (minimised) is the minimised energy of the isolated receptor. The three main contributions that we considered are: ΔG_{MM} (molecular mechanics interaction), ΔG_{PB} (polar solvation energy), and ΔG_{SA} (nonpolar solvation energy), to obtain DGbind. The term ΔG_{MM} considers the amount of electrostatic + van der Waals. The ΔG_{PB} and the ΔG_{SA} parameters correspond to the solvation energies' nonpolar and polar expressions.

With an average binding energy of -127.6 kcal/mol, Compound 90 exhibited the strongest binding affinity among all tested ligands. In contrast, compound 1CJS and Compound 175 showed substantially weaker affinities, at -33.2 and -31.3 kcal/mol, respectively, while the natural ligand GTP displayed a binding affinity of -89.9 kcal/mol (Table 4). These findings indicate that Compound 90 interacts with the active site far more strongly than both the native ligand and the other evaluated compounds.

Compound 90's much greater binding indicates that it may be a powerful RdRp inhibitor and competitive GTP mimic. MD modelling results confirm that it can efficiently occupy and stabilise the catalytic site. All these results point to Compound 90 as a promising antiviral candidate for more dengue virus research.

Table 4
MM/PBSA free energy of binding (kcal/mol)

Ligand	MM/PBSA kcal/mol
90	-127.6
1CJS	-33.2
175	-31.3
GTP (control)	-89.9

Binding Mechanism of Compound 90

Hydrogen bonds and hydrophobic interactions are crucial for ligand-protein complex stabilisation and binding affinity determination in computational drug development. In order to fix ligands at the binding site, hydrogen bonds, which are created between a hydrogen atom and electronegative atoms like oxygen or nitrogen, are essential. The stability of the complex is greatly increased by these interactions, which also improve binding specificity.

Tight binding within hydrophobic pockets is promoted by hydrophobic interactions, which happen when non-polar parts of the ligand and protein group together to avoid water. Supported by van der Waals forces, these interactions enhance total affinity and help keep the ligand oriented correctly. When combined, these pressures are essential for assessing and improving ligand binding during the drug discovery process.

The binding behaviour of compound 90 within the active site of DENV RdRp over a 150-ns molecular dynamics simulation is shown in Figure 11. The ligand demonstrated stable and specific binding, characterised by a network of hydrophobic contacts and hydrogen bonds that contributed to its strong affinity and conformational stability. Among the interacting residues, Arg729 emerged as the most critical, maintaining both hydrogen bonding and hydrophobic interactions for over 70% of the simulation time. This persistent engagement anchored the ligand effectively within the binding pocket, enhancing specificity and minimising positional drift.

Trp795 also played a significant role, forming consistent hydrophobic interactions (~71%) with the ligand's nonpolar region, likely through favourable van der Waals forces that further stabilised the complex. Additionally, residues Asp663 and Asp664 provided moderate support via transient hydrogen bonds and hydrophobic contacts, likely aiding in optimal ligand orientation. Interactions with Ser710 and Thr794 were less frequent, reflecting the inherent flexibility of nearby loop regions and the dynamic nature of the binding site.

Despite the variability in individual residue contributions, Compound 90 established a residue-specific interaction pattern, primarily anchored by Arg729 and Trp795, that maintained a stable and favourable pose throughout the trajectory.

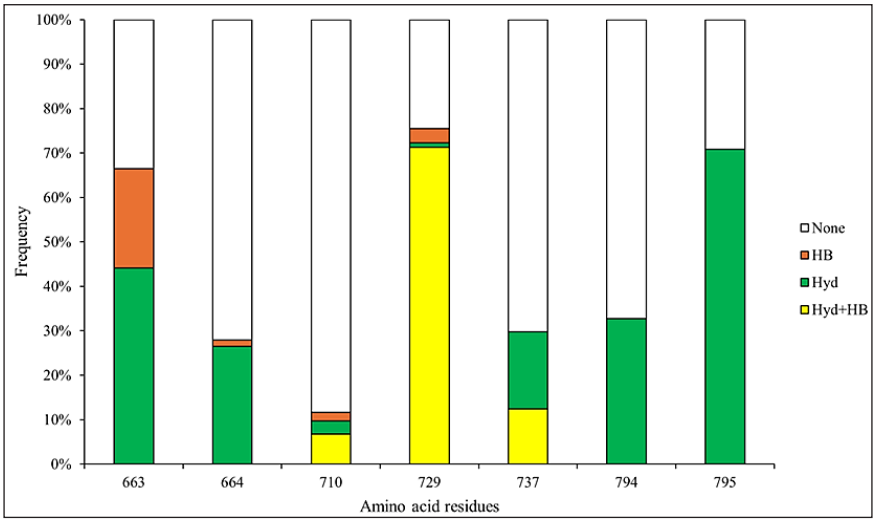

Figure 11. Frequency distribution of interactions between compound 90 and selected amino acid residues of RdRp during the 150 ns MD simulation

The MM/PBSA-calculated binding free energy of -127.6 kcal/mol further reinforces its strong binding affinity, exceeding that of the native ligand GTP and other tested compounds. These results underscore Compound 90's potential as a potent RdRp inhibitor and a promising candidate for antiviral drug development.

The 150-ns molecular dynamics simulation of the native ligand, revealing a stable binding profile predominantly maintained through hydrophobic interactions (Figure 12). Key residues such as Arg737, Thr794, and Trp795 consistently formed strong nonpolar contacts, indicating that the ligand was securely anchored within a hydrophobic pocket. These interactions, primarily mediated by van der Waals forces, contributed to a fixed ligand conformation and limited positional fluctuation features essential for maintaining binding stability.

The native ligand showed less hydrogen bonding than compound 90, which led to a less varied network of interactions. Interestingly, Asp663 and Asp664 showed minimal to no involvement, most likely as a result of peripheral placement in relation to the ligand or suboptimal spatial orientation. More prominent hydrophobic contacts maintained the overall stability of the binding even in their absence. Occasionally, Ser710 created hydrogen bonds, which provided slight polar stability without having a major impact on the orientation of the ligand.

Although less interactive than compound 90, the native ligand maintained steady contact with critical residues, affirming its role as a stable, albeit less optimised, binder. These findings highlight the native ligand's sufficient binding stability while emphasising the superior interaction profile of compound 90.

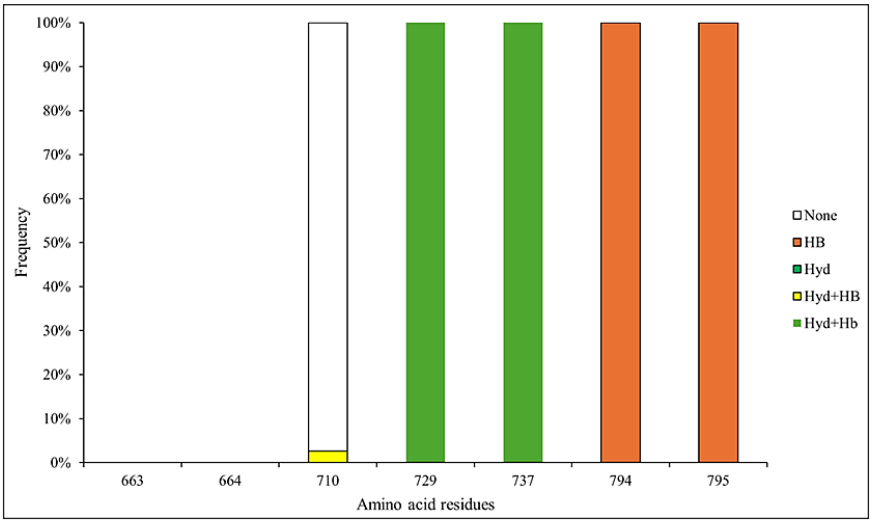

Figure 12. Frequency distribution of interactions between native ligand and selected amino acid residues of RdRp during the 150 ns MD simulation.

Curcumin has long been recognised for its broad antiviral properties, including activity against dengue virus. Previous studies showed that, at low concentrations (10-30 μM), curcumin reduces viral replication not by directly targeting viral enzymes but by affecting host-cell processes such as the actin cytoskeleton and the ubiquitin-proteasome system, leading to accumulation of viral proteins and reduced plaque formation (Padilla-S et al., 2014). Structural studies also revealed that curcumin can allosterically inhibit the NS2B–NS3 protease by binding to a non-active site cavity and destabilising its active conformation (Lim et al., 2020). However, these effects are relatively moderate and indirect. In our study, compound 90 showed a markedly different profile. It directly binds to the dengue RNA-dependent RNA polymerase RdRp, forming stable interactions with key catalytic residues, and molecular dynamics analyses demonstrated that it closely mimics the native ligand GTP in both structure and dynamic behaviour. Compound 90 combines strong specificity with potent inhibitory potential, directly interfering with viral replication. These findings suggest that rationally designed curcuminoids, such as compound 90, can overcome the limitations of native curcumin and represent promising leads for the development of more effective dengue antivirals.

CONCLUSION

In this study, we used computational approaches to identify potential inhibitors of dengue virus RdRp. Molecular dynamics simulations of 150 ns were performed to evaluate the stability and interactions of both apoprotein and ligand-bound RdRp. Ensemble docking of 328 curcuminoid compounds yielded three promising hits, with compound 90 emerging

as the strongest candidate, showing the highest binding affinity even surpassing the native ligand GTP. Post-simulation analyses, including RMSD, RMSF, radius of gyration, PCA, DCCM, and MM/PBSA, confirmed its stable binding and revealed that it closely mimics the dynamic behaviour of GTP within the active site, suggesting it could act as a competitive or pseudo-substrate inhibitor. Compound 90 formed persistent hydrogen bonds with key residues, including Ser710, Arg737, Thr794, Trp795, and the catalytic Asp663 and Asp664, which remained stable throughout the simulation. These results highlight Compound 90 as a highly promising RdRp inhibitor and support its further experimental validation as a potential antiviral agent against dengue virus.

ACKNOWLEDGEMENT

The authors would like to thank Priya Murugan and Yuan Chongjun for technical assistance. This research received no external funding.

REFERENCES

Adkins, J. C., & Faulds, D. (1998). Amprenavir. *Drugs, 55*(6), 837-842. https://doi.org/10.2165/00003495-199855060-00015

Balasubramanian, A., Pilankatta, R., Teramoto, T., Sajith, A. M., Nwulia, E., Kulkarni, A., & Padmanabhan, R. (2019). Inhibition of dengue virus by curcuminoids. *Antiviral Research, 162*, 71-78. https://doi.org/10.1016/j.antiviral.2018.12.002

Berman, H. M., Westbrook, J., Feng, Z., Gilliland, G., Bhat, T. N., Weissig, H., Shindyalov, I. N., & Bourne, P. E. (2000). The Protein Data Bank. *Nucleic Acids Research, 28*(1), 235-242. https://doi.org/10.1093/nar/28.1.235

Brooks, B. R., Bruccoleri, R. E., Olafson, B. D., States, D. J., Swaminathan, S., & Karplus, M. (1983). CHARMM: A program for macromolecular energy, minimization, and dynamics calculations. *Journal of Computational Chemistry, 4*(2), 187-217. https://doi.org/10.1002/jcc.540040211

Douglas, W. W., & Rubin, R. P. (1961). The role of calcium in the secretory response of the adrenal medulla to acetylcholine. *The Journal of Physiology, 159*(1), 40-57. https://doi.org/10.1113/jphysiol.1961.sp006791

Hassan, H. A., Hassan, A. R., Mohamed, E. A. R., Al-Khdhairawi, A., Karkashan, A., Attar, R., Allemailem, K. S., Abdulmonem, W. Al, Shimizu, K., Abdel-Rahman, I. A. M., & Allam, A. E. (2022). Conducting the RBD of SARS-CoV-2 Omicron variant with phytoconstituents from *Euphorbia dendroides* to repudiate the binding of spike glycoprotein using computational molecular search and simulation approach. *Molecules, 27*(9), Article 2929. https://doi.org/10.3390/molecules27092929

Khetarpal, N., & Khanna, I. (2016). Dengue fever: Causes, complications, and vaccine strategies. *Journal of Immunology Research, 2016*, Article 6803098. https://doi.org/10.1155/2016/6803098

Krieger, E., & Vriend, G. (2015). New ways to boost molecular dynamics simulations. *Journal of Computational Chemistry, 36*(13), 996-1007. https://doi.org/10.1002/jcc.23899

Lim, L., Dang, M., Roy, A., Kang, J., & Song, J. (2020). Curcumin allosterically inhibits the dengue NS2B-NS3 protease by disrupting its active conformation. *ACS Omega, 5*(40), 25677-25686. https://doi.org/10.1021/acsomega.0c00039

Lim, S. P., Noble, C. G., Nilar, S., Shi, P.-Y., & Yokokawa, F. (2018). Discovery of potent non-nucleoside inhibitors of dengue viral RNA-dependent RNA polymerase from fragment screening and structure-guided design. In *Methods in molecular biology* (pp. 187-198). https://doi.org/10.1007/978-981-10-8727-1_14

Mahmood, K., Zia, K. M., Zuber, M., Salman, M., & Anjum, M. N. (2015). Recent developments in curcumin and curcumin-based polymeric materials for biomedical applications: A review. *International Journal of Biological Macromolecules, 81*, 877-890. https://doi.org/10.1016/j.ijbiomac.2015.09.026

Maier, J. A., Martinez, C., Kasavajhala, K., Wickstrom, L., Hauser, K. E., & Simmerling, C. (2015). ff14SB: Improving the accuracy of protein side chain and backbone parameters from ff99SB. *Journal of Chemical Theory and Computation, 11*(8), 3696-3713. https://doi.org/10.1021/acs.jctc.5b00255

Markham, A. (2017). Baricitinib: First global approval. *Drugs, 77*(6), 697-704. https://doi.org/10.1007/s40265-017-0723-3

Martínez-Rosell, G., Giorgino, T., & De Fabritiis, G. (2017). PlayMolecule ProteinPrepare: A web application for protein preparation for molecular dynamics simulations. *Journal of Chemical Information and Modeling, 57*(7), 1511-1516. https://doi.org/10.1021/acs.jcim.7b00190

O'Boyle, N. M., Banck, M., James, C. A., Morley, C., Vandermeersch, T., & Hutchison, G. R. (2011). Open Babel: An open chemical toolbox. *Journal of Cheminformatics, 3*(1), Article 33. https://doi.org/10.1186/1758-2946-3-33

Padilla-S, L., Rodríguez, A., Gonzales, M. M., Gallego-G, J. C., & Castaño-O, J. C. (2014). Inhibitory effects of curcumin on dengue virus type 2-infected cells in vitro. *Archives of Virology, 159*(3), 573-579. https://doi.org/10.1007/s00705-013-1849-6

Prlina, I. M., Dahlen, C. P., & Bischoff, A. J. (1958). Sulfamethoxypyridazine, a new sulfonamide for urinary infections: A preliminary report. *Antibiotic Medicine & Clinical Therapy (New York, NY), 5*(4), 242-250.

Qureshi, A. I. (2020). Dengue virus infection. In A. I. Qureshi (Ed.), *Dengue virus disease* (1st ed., pp. 1-7). Elsevier. https://doi.org/10.1016/B978-0-12-818270-3.00001-1

Singh, P. K., Pathania, S., & Rawal, R. K. (2020). Exploring RdRp-remdesivir interactions to screen RdRp inhibitors for the management of novel coronavirus 2019-nCoV. *SAR and QSAR in Environmental Research, 31*(11), 857-867. https://doi.org/10.1080/1062936X.2020.1825014

Siviero, A., Gallo, E., Maggini, V., Gori, L., Mugelli, A., Firenzuoli, F., & Vannacci, A. (2015). Curcumin, a golden spice with a low bioavailability. *Journal of Herbal Medicine, 5*(2), 57-70. https://doi.org/10.1016/j.hermed.2015.03.001

Stroganov, O. V., Novikov, F. N., Stroylov, V. S., Kulkov, V., & Chilov, G. G. (2009). ChemInform abstract: Lead Finder: An approach to improve accuracy of protein-ligand docking, binding energy estimation, and virtual screening. *ChemInform, 40*(16), Article 119992. https://doi.org/10.1002/chin.200916212

Weaver, S. C., & Vasilakis, N. (2009). Molecular evolution of dengue viruses: Contributions of phylogenetics to understanding the history and epidemiology of the preeminent arboviral disease. *Infection, Genetics and Evolution, 9*(4), 523-540. https://doi.org/10.1016/j.meegid.2009.02.003

Yap, T. L., Xu, T., Chen, Y.-L., Malet, H., Egloff, M.-P., Canard, B., Vasudevan, S. G., & Lescar, J. (2007). Crystal structure of the dengue virus RNA-dependent RNA polymerase catalytic domain at 1.85-angstrom resolution. *Journal of Virology, 81*(9), 4753-4765. https://doi.org/10.1128/JVI.02283-06